Research on Chemical Intermediates
https://doi.org/10.1007/s11164-019-03838-9

Quantum chemical, experimental, theoretical spectral (FT-IR and NMR) studies and molecular docking investigation of 4,8,9,10-tetraaryl-1,3-diazaadamantan-6-ones

G. Vengatesh[1] · M. Sundaravadivelu[1]

Received: 2 March 2019 / Accepted: 16 April 2019

Abstract

The compounds 4,8,9,10-tetraaryl-1,3-diazaadamantan-6-ones (**a**–**e**) were synthesized and characterized by FT-IR, ^{1}H and ^{13}C NMR spectra, and the spectral data have been theoretically analyzed by the DFT method. The electronic properties including a highest occupied molecular orbital (HOMO), lowest unoccupied molecular orbital (LUMO) and related parameters were calculated with B3LYP/6-311 G (d, p) basis set. The observed HOMO and LUMO mappings describe the different charge transfer possibilities within the molecule. Besides, the reactive properties of the molecules have been addressed based on the frontier molecular orbital analysis. The Molecular Electrostatic Potential and Fukui function analysis reveal the sites for electrophilic attack and nucleophilic reactions in the molecule. The intramolecular contacts have been interpreted using Natural Bond Orbital analysis and the thermodynamic properties also presented. The molecular docking study has been executed to study the binding interactions of the synthesized compounds with H1N1 swine virus-M2 proton channel and COX-2 protein.

Electronic supplementary material The online version of this article (https://doi.org/10.1007/s11164-019-03838-9) contains supplementary material, which is available to authorized users.

✉ M. Sundaravadivelu
msundargri@gmail.com

[1] Department of Chemistry, The Gandhigram Rural Institute-Deemed to be University, Gandhigram, Tamilnadu 624 302, India

Published online: 26 April 2019

Graphical abstract

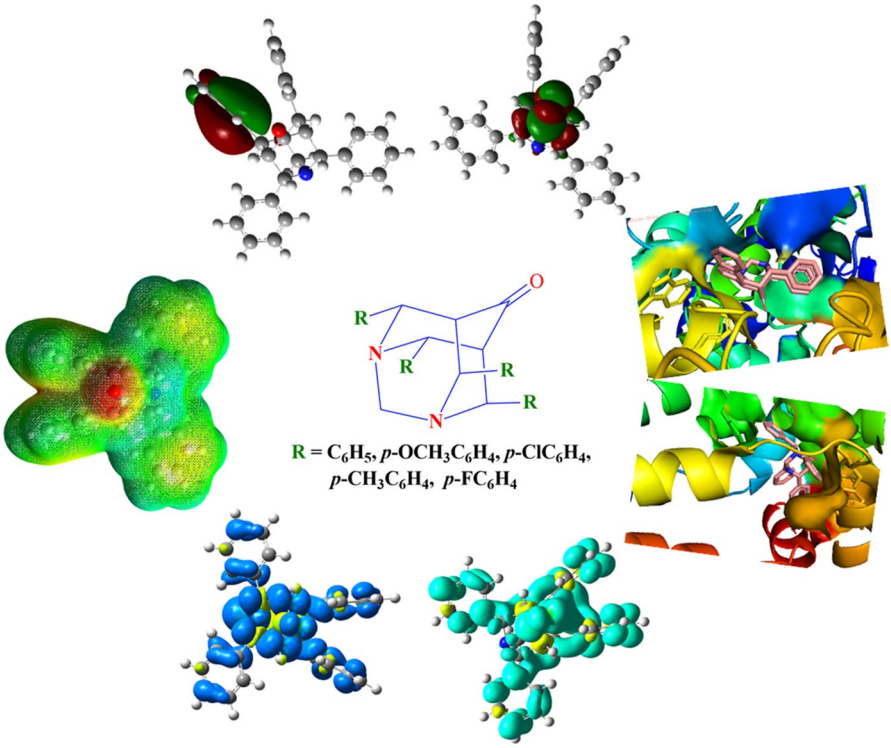

Keywords 1,3 diazaadamantanone · Fukui function · MEP · NBO · NMR · Molecular docking

Introduction

The biological activities of adamantane core containing compounds were early recognized after the discovery of amantadine and its derivatives as effective therapies against influenza viruses [1–4]. Since they have intensive biological properties, several drugs containing adamantane core have been discovered, which are now available in the market, Fig. 1. Furthermore, several adamantane derivatives were proved to possess potent biological activities against human immunodeficiency viruses (HIV) [5, 6], anti-inflammatory [7–9], central nervous activities [10–12], anti-diabetic [13, 14] and anti-microbial [15–19]. The 1,3 diazaadamantanone core containing derivatives are of great importance as conformationally rigid analogs of medicinally active compounds. This derivative has great antimicrobial activities [20]. In view of vast varieties of biological activities of adamantane derivatives, we synthesized five tetraaryl substituted 1,3 diazaadamantanone derivatives, namely 4,8,9,10-tetraaryl-1,3-diazaadamantan-6-ones.

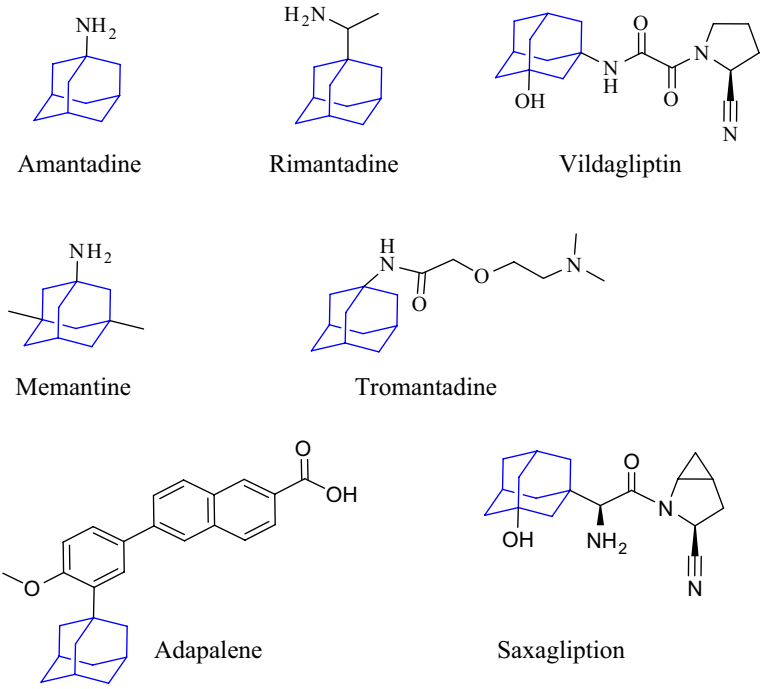

Fig. 1 Available adamantane core containing drugs

The literature review revealed that synthesis and conformational studies of the 4,8,9,10-tetraaryl-1,3-diazaadamantan-6-one were carried out using NMR and XRD [21, 22].

In the literature, to the best of our insight, there is no DFT and docking study done for the title compound. The biological activities of the compounds are based on the electronic properties of the molecule (HOMO, LUMO, dipole movement, total energy, etc.). In this investigation, the electronic properties of five tetraaryl substituted 1,3 diazaadamantanones have been studied using density functional theory, a B3LYP method with 6-311 G (d, p) basis set. The frontier molecular orbitals such as HOMO and LUMO determine the way the molecule interacts with other species which enables us to characterize the chemical reactivity of the molecule. The stability of the molecule arising from hyper-conjugative interaction and charge delocalization has been analyzed using Natural Bonding Orbital (NBO) analysis and Molecular Electrostatic Potential (MEP) analysis. The current investigation also deals with molecular docking study of the five 4,8,9,10-tetraaryl-1,3-diazaadamantan-6-one in H1N1 swine viruses and COX-2 protein.

Experimental details

The synthesis and crystal structure of the studied 4,8,9,10-tetraaryl-1,3-diazaadamantan-6-ones (**a–e;** Fig. 2) have been reported earlier [21, 22]. In this investigation, five 4,8,9,10-tetraaryl-1,3-diazaadamantan-6-ones (**a–e**) are synthesised and compounds are confirmed by spectral techniques. The FT-IR spectra had been recorded using a JASCO FT/IR-4700 spectrometer in the region 4000–400 cm^{-1} as a KBr pellet. The ^{1}H and ^{13}C NMR spectra were recorded in a Bruker AVANCER III HD 400 MHz instrument at 300 K. The compound was dissolved in $CDCl_3$ and chemical shifts are reported in ppm relative to tetramethyl silane (TMS). The ^{1}H and ^{13}C NMR spectra had been recorded at a base frequency of 400 MHz and 100 MHz, respectively. Synthesis procedure for the compounds (**a–e**) and their FT-IR and NMR spectra are shown in the supporting information.

General procedure for the synthesis of compounds (a–e)

Compounds 1−5 were synthesised by the methods reported in literature [21, 22]. The compound **1–5** (1 mmol) was dissolved in chloroform and 2 mmol of paraformaldehyde was added. The mixture was refluxed and monitored by TLC. After the complete disappearance of the starting material, there was evaporation of the solvent

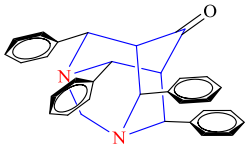

4,8,9,10-tetraphenyl-1,3-diazaadamantan-6-one **(a)**

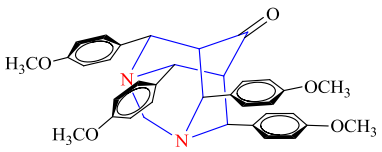

4,8,9,10-tetrakis(4-methoxyphenyl)-1,3--diazaadamantan-6-one **(b)**

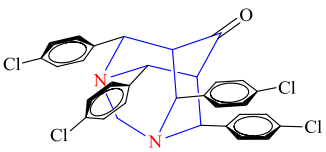

4,8,9,10-tetrakis(4-chlorophenyl)-1,3--diazaadamantan-6-one **(c)**

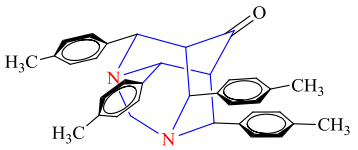

4,8,9,10-tetra-*p*-tolyl-1,3-diazaadamantan-6-one **(d)**

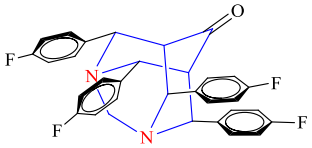

4,8,9,10-tetrakis(4-fluorophenyl)-1,3--diazaadamantan-6-one **(e)**

Fig. 2 Structure of the synthesized compound **a–e**

in the resulting mixture, and it was washed with cold water to obtain colorless solid as a resulting product (Scheme 1).

4,8,9,10-tetraphenyl-1,3-diazaadamantan-6-one (**a**); Colorless power, mp 210 °C; IR (KBr, cm^{-1}): 3086, 3054, 3027. 2982, 2951, 2878, 1705, 1601; ^{1}H-NMR ($CDCl_3$/TMS, 400.22 MHz) 3.98 (2H, s), 4.44 (2H, s), 4.76 (2H, s), 4.85 (2H, s), 6.77 (6H, m), 7.02 (4H, d), 7.30 (2H, t), 7.40 (4H, t), 7.61 (4H, d). ^{13}C-NMR ($CDCl_3$/TMS, 100.63 MHz) 50.17, 64.26, 68.55, 69.42, 126.36, 126.96, 127.31, 127.51, 128.10, 129.10, 138.00, 139.66, 213.70.

4,8,9,10-tetrakis(4-methoxyphenyl)-1,3-diazaadamantan-6-one (**b**); Colorless power, mp 188 °C; IR (KBr, cm^{-1}): 3066, 3034, 2992, 2953, 2903, 2866, 2833, 1695, 1608; ^{1}H-NMR ($CDCl_3$/TMS, 400.22 MHz) 3.63 (6H, s), 3.82 (6H, s), 3.87 (2H, s), 4.36 (2H, s), 4.67 (2H, s), 4.81 (2H, s), 6.36 (4H, d), 6.92 (8H, m), 7.50 (4H, d). ^{13}C-NMR ($CDCl_3$/TMS, 100.63 MHz) 50.48, 55.19, 55.31, 63.57, 67.89, 68.97, 112.87, 114.35, 128.10, 129.18, 130.03, 132.39, 157.70, 158.81, 214.15.

4,8,9,10-tetrakis(4-chlorophenyl)-1,3-diazaadamantan-6-one (**c**); Colorless power, mp 198 °C; IR (KBr, cm^{-1}): 3083, 3048, 2947, 2892, 2875, 1705, 1593; ^{1}H-NMR ($CDCl_3$/TMS, 400.22 MHz) 3.85 (2H, s), 4.34 (2H, s), 4.69 (2H, s), 4.73 (2H, s), 6.84 (4H, s), 6.90 (4H, s), 7.41 (4H, s), 7.50 (4H, s). ^{13}C-NMR ($CDCl_3$/TMS, 100.63 MHz) 49.76, 63.56, 68.15, 68.58, 127.57, 128.26, 129.42, 132.82, 133.67, 135.94, 137.63, 212.25.

4,8,9,10-tetra-p-tolyl-1,3-diazaadamantan-6-one (**d**); Colorless power, mp 211 °C; IR (KBr, cm^{-1}): 3051, 3022, 2958, 2916, 2882, 2860, 1701, 1514; ^{1}H-NMR ($CDCl_3$/TMS, 400.22 MHz) 2.08 (6H, s), 2.36 (6H, s), 3.90 (2H, s), 4.38 (2H, s), 4.68 (2H, s), 4.81 (2H, s), 6.59 (4H, d), 6.85 (4H, d), 7.19 (4H, d), 7.47 (4H, d).

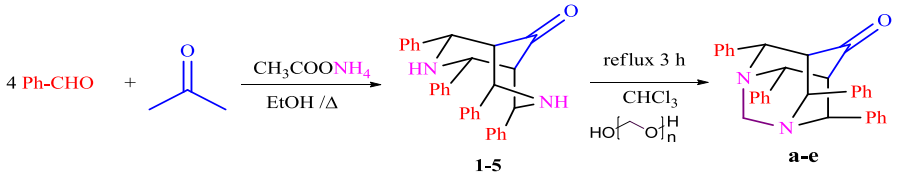

Compounds	Ph	Yield %
a	C_6H_5	88
b	*p*-OCH_3 C_6H_4	80
c	*p*-Cl C_6H_4	89
d	*p*-CH_3 C_6H_4	82
e	*p*-F C_6H_4	90

Scheme 1 Synthesis of compound **a**–**e**

^{13}C-NMR ($CDCl_3$/TMS, 100.63 MHz) 20.78, 21.11, 50.42, 63.93, 68.25, 69.35, 126.90,127.84, 128.04, 129.72, 135.13, 135.68, 136.98, 137.08, 214.20.

4,8,9,10-tetrakis(4-fluorophenyl)-1,3-diazaadamantan-6-one (**e**); Colorless power, mp 236 °C; IR (KBr, cm^{-1}): 3062, 3045, 2947, 2885, 1705, 1601; ^{1}H-NMR ($CDCl_3$/TMS, 400.22 MHz) 3.87 (2H, s), 4.36 (2H, s), 4.70 (2H, s), 4.78 (2H, s), 6.54 (4H, s), 6.97 (4H, s), 7.12 (4H, s), 7.55 (4H, s). ^{13}C-NMR ($CDCl_3$/TMS, 100.63 MHz) 50.00, 63.47, 68.02, 68.62, 114.11, 114.32, 115.98, 116.20, 128.52, 128.60, 129.66, 129.74, 133.23, 133.26, 135.24, 135.27, 160.04, 160.90, 162.49, 163.36, 212.73.

Computational details

The theoretical calculations of the studied compounds are carried out with the Gaussian 09 W software package using the Becke's three-parameter hybrid exchange function with the LeeYang-Parr (LYP) correlation function (B3LYP) method. The molecular structure of 4,8,9,10-tetraaryl-1,3-diazaadamantan-6-ones in the ground state was optimized using Density Functional Theory (DFT). The optimized structure and other electronic properties had been pursued by the Gauss View 5.0 program. The electronic properties such as Highest Occupied Molecular Orbital (HOMO) and Lowest Unoccupied Molecular Orbital (LUMO), HOMO–LUMO energy gap (ΔE), ionization potential (I), electron affinity (A), electronegativity (χ), global hardness (η) and global softness (σ) were computed using the E_{HOMO} and E_{LUMO} energies at the B3LYP/6–311 G (d, p) level of theory. The Molecular Electrostatic Potential (MEP) map also was viewed using the Gauss View 5.0 program. The Natural Bond Orbital (NBO) was calculated on the studied compounds at the B3LYP level utilizing the basis set 6-311 G (d, p).

Assessment of the binding affinities of H1N1 swine virus M2 proton channel and cyclooxygenase-2 (COX-2) protein in the synthesized compounds was done with molecular docking simulation. The docking simulation was achieved using the Auto dock 4.2.6 software program to predict the protein–ligand interactions. Initially, the structure of 1,3 diazaadamantanones was optimized with minimizing its energy at B3LYP/6-311 G (d, p) level of theory. The 3D X-ray crystal structure of the H1N1–M2 proton channel and COX-2 were acquired from the protein data bank (http://www.rcsb.org; PDB ID: 2RLF, 4COX) [23, 24]. The downloaded protein structures were cleaned by removing water and co-crystallised ligands. The active site of the enzyme was defined to include active sites of the residues within the grid size of 100 Å × 100 Å × 70 Å and 60 Å × 60 Å × 60 Å in H1N1–M2 proton channel and COX-2 protein, respectively. The most popular Lamarckian Genetic Algorithm (LGA) was employed for docking [25]. As required in the LGA, polar hydrogen atoms and Kolhman charges were added to the structure of proteins by using the Auto Dock Tools (ADT). The binding site of the ligand–protein was viewed by the molecular graphics software of PYMOL and UCSF Chimera.

Result and discussion

FT-IR spectral study

The calculated wavenumber and observed FT-IR frequency of the compound **a-e** are given in Table 1. In the following discussion, the compound **a** is taken as a representative compound. The asymmetric and symmetric CH stretching frequency of the aromatic phenyl rings appeared at 3086–3026 cm^{-1}, the calculated frequency appeared at 3212–3133 cm^{-1}. Aliphatic asymmetric and symmetric CH stretching frequency of the diazaadamantan-6-one appeared in the range of 2982–2878 cm^{-1}, and the theoretically calculated frequency appeared at 3132–3033 cm^{-1}. Strong adsorption bands in the vicinity of the 1705 cm^{-1} in the experimental FT-IR spectrum of the representative compound are assigned to the C=O stretching with calculated scaled wavenumber 1710 cm^{-1}. The aromatic asymmetric and symmetric C=C stretching frequency appeared at 1601 cm^{-1}, the theoretically calculated frequency appeared at 1545 cm^{-1}. Correlation between the experimental and calculated wavenumbers are obtained by plotting a correlation graph of compounds **a**–**e** and are given in supporting information. The result shows a good linear correlation with the calculated wavenumbers. The correlation equation and linear correlation coefficients (R^2) are given in Table S1.

NMR spectral study

The experimental ^{1}H NMR spectrum for compound **a**–**e** in $CDCl_3$ solvent is given in supporting information. The optimized molecular structures of compound **a**–**e** were used to stimulate ^{1}H NMR spectrum at DFT/B3LYP 6311G (d, p) level using the gauge-independent atomic orbital (GIAO) method and computed ^{1}H and ^{13}C NMR spectra are shown in supporting information in Table S2, S3 [26, 27]. The predicted proton chemical shifts are in good agreement with the experimental data. The compound **a** is taken as a representative compound for experimental ^{1}H and ^{13}C NMR spectral discussion. The one pair of benzylic protons H-4 and 10 appeared in the range of δ 4.85 ppm, another pair of benzylic protons H-8 and 9 appeared at δ 4.76 ppm. The H-4 and 10 protons that appeared in the upfield region are due to parallel orientation of C-8 and 9 phenyl groups (ring current effect). The bridgehead (H-5 & 7) and piperidine nitrogen bridging protons (H-2) appeared at δ 3.98 and 4.44 ppm, respectively. The aromatic protons appeared at δ 6.77–7.63 ppm.

The correlation graph of compounds is given in supporting information. The correlation graph is drawn between the experimental and calculated chemical shifts values of the compounds **a**–**e**. The relations between the experimental and calculated chemical shifts values equations are given in Table 2. In all the five compounds, the ^{13}C NMR calculations gave better linear correlation coefficients (R^2) than for ^{1}H NMR chemical shift. A small deviation between the experimental and computed chemical shifts of these compounds are noted, and this may be due to the orientation and stereochemistry of the aryl groups.

Table 1 Calculated and experimental FT-IR frequency (cm^{-1}) of compounds **a**–**e**

Compounds	**a** Exp.	**a** Cal.	**b** Exp.	**b** Cal.	**c** Exp.	**c** Cal.	**d** Exp.	**d** Cal.	**e** Exp.	**e** Cal.
C=O	1705	1710	1695	1701	1705	1866	1701	1702	1705	1702
Aromatic C=C	1601	1545	1608	1591	1593	1563	1514	1592	1601	1582
Aromatic CH	3086–3027	3212–3133	3066–3034	3246–3145	3083–3048	3250–3147	3051–3022	3248–3146	3062–3045	3247–3146
Aliphatic CH, CH_2	2982–2878	3133–3033	2992–2833	3103–3033	2947–2875	3113–3045	2958–2860	3112–3044	2947–2885	3112–3044

Table 2 Relations between the experimental and calculated chemical shifts of compounds **a–e**

Compounds	Analysis	R^2	Correlation equations
a	^{1}H NMR	0.9596	$\delta_{cal} = 1.0869\ \delta_{exp} - 0.6069$
	^{13}C NMR	0.9863	$\delta_{cal} = 1.0234\ \delta_{exp} + 12.9751$
b	^{1}H NMR	0.9754	$\delta_{cal} = 1.1253\ \delta_{exp} - 0.9446$
	^{13}C NMR	0.9793	$\delta_{cal} = 0.9838\ \delta_{exp} + 12.5073$
c	^{1}H NMR	0.9746	$\delta_{cal} = 1.1163\ \delta_{exp} - 0.8815$
	^{13}C NMR	0.9954	$\delta_{cal} = 1.0107\ \delta_{exp} + 12.9282$
d	^{1}H NMR	0.9877	$\delta_{cal} = 1.1240\ \delta_{exp} - 0.7669$
	^{13}C NMR	0.9968	$\delta_{cal} = 1.0141\ \delta_{exp} + 12.3283$
e	^{1}H NMR	0.9835	$\delta_{cal} = 1.1524\ \delta_{exp} - 0.9654$
	^{13}C NMR	0.6561	$\delta_{cal} = 0.9570\ \delta_{exp} + 15.9153$

Thermodynamic study

Table 3, indicates thermodynamic parameters of compounds **a-e**. Mentioned parameters for each molecule are calculated by using B3LYP/6-311G (d, p) basis set. The frequency calculations are to determine the zero-point energies, Gibbs-free energies, enthalpy, entropy, as well as the heat capacity for a molecular system. A higher value of Gibbs-free energies implies more stable molecules. The stability order of the studied compound is **b > d > a > e > c**, indicating that compounds with electron donating groups are more stable compared to compounds with electron withdrawing groups. The values of enthalpy, entropy zero-point vibrational energy and heat capacity can be obtained at any temperature and are useful in estimating the direction of chemical reactions. The results of the free energy, entropy, enthalpy, and zero-point vibrational energy can be used for synthesis of new molecules which include tetraaryl 1,3-diazaadamantan derivatives.

Frontier molecular orbital analysis

The optimized geometry of the compounds **a–e** is illustrated in Fig. 3. Both the highest occupied molecular orbital (HOMO) and lowest unoccupied molecular

Table 3 Theoretically computed thermodynamic parameters of the title compound employing B3LYP/6-311G (d, p) basis set

Compounds	**a**	**b**	**c**	**d**	**e**
Enthalpy (hartrees)	0.5528	0.6924	0.5185	0.6706	0.5226
Gibbs free energy (hartrees)	0.4684	0.6017	0.4376	0.5800	0.4457
Zero-point vibrational energy (k cal mol^{-1})	329.90	415.59	309.23	403.00	312.64
Heat capacity (cal mol^{-1} K^{-1})	108.38	124.71	107.00	115.81	103.93
Entropy (cal mol^{-1} K^{-1})	177.52	190.82	170.29	190.61	161.73

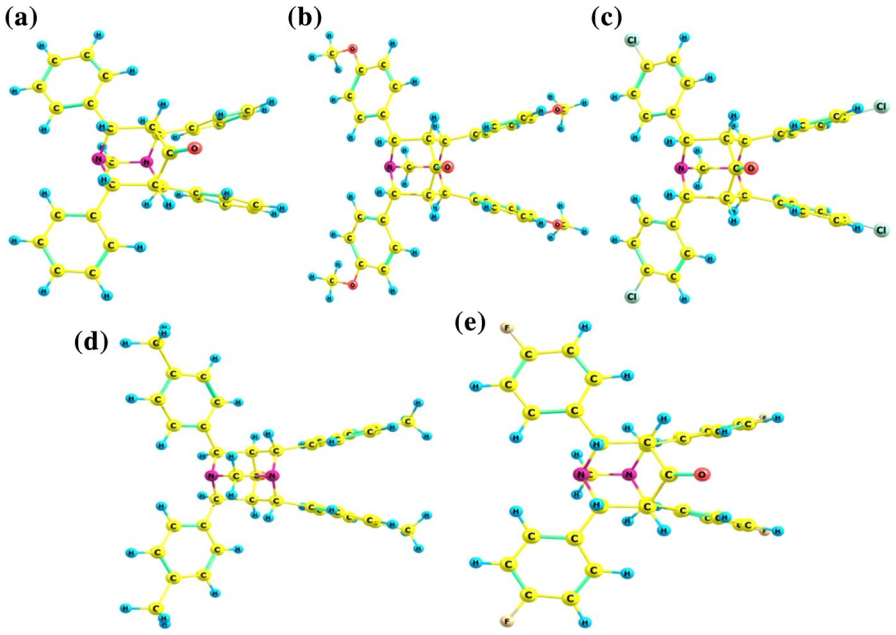

Fig. 3 Optimized geometry (B3LYB/6-311 G (d, p) (5D, 7F)) of synthesized compounds **a**–**e**

orbital (LUMO) and their properties are very useful for a chemical reaction. The HOMO, HOMO-1, LUMO and LUMO + 1 plots of the studied molecules are shown in Fig. 4. In the title compounds (**a**–**e**), HOMO is located over any one of the axially oriented aryl rings and LUMO is located over the carbonyl group. In the case of compound **c,** LUMO is located in one of the equatorially orientated aryl rings. The higher value of HOMO indicates the ability of the molecule to donate electrons to an appropriate acceptor molecule and a lower value of LUMO indicates the ability of the molecule to accept electrons for an appropriate donor molecule. From Table 4, it is evident that the HOMO for the title compound increased in the order **b** (*p*-OCH_3), **d** (*p*-CH_3), **a** (H), **e** (*p*-F), **c** (*p*-Cl). This result reveals that the electron donating group increases the nucleophilicity of the molecule. In the case of LUMO, the order decreases **c**, **e**, **a**, **d** and **b**. This result reveals that the electron withdrawing group increases the electrophilicity of the molecule. The energy of HOMO is directly related to the ionization potential (*I*) and LUMO energy is directly related to the electron affinity (*A*) of the molecule [28]. The global chemical reactivity descriptors such as hardness, softness, chemical potential, electronegativity, and electrophilicity are calculated using the HOMO and LUMO values. These parameters are calculated using the following equations [29–32], and the corresponding values for the compounds (**a**–**e**) are presented in Table 4.

$$I = -E_{\mathrm{HOMO}} \tag{1}$$

$$A = -E_{\mathrm{LUMO}} \tag{2}$$

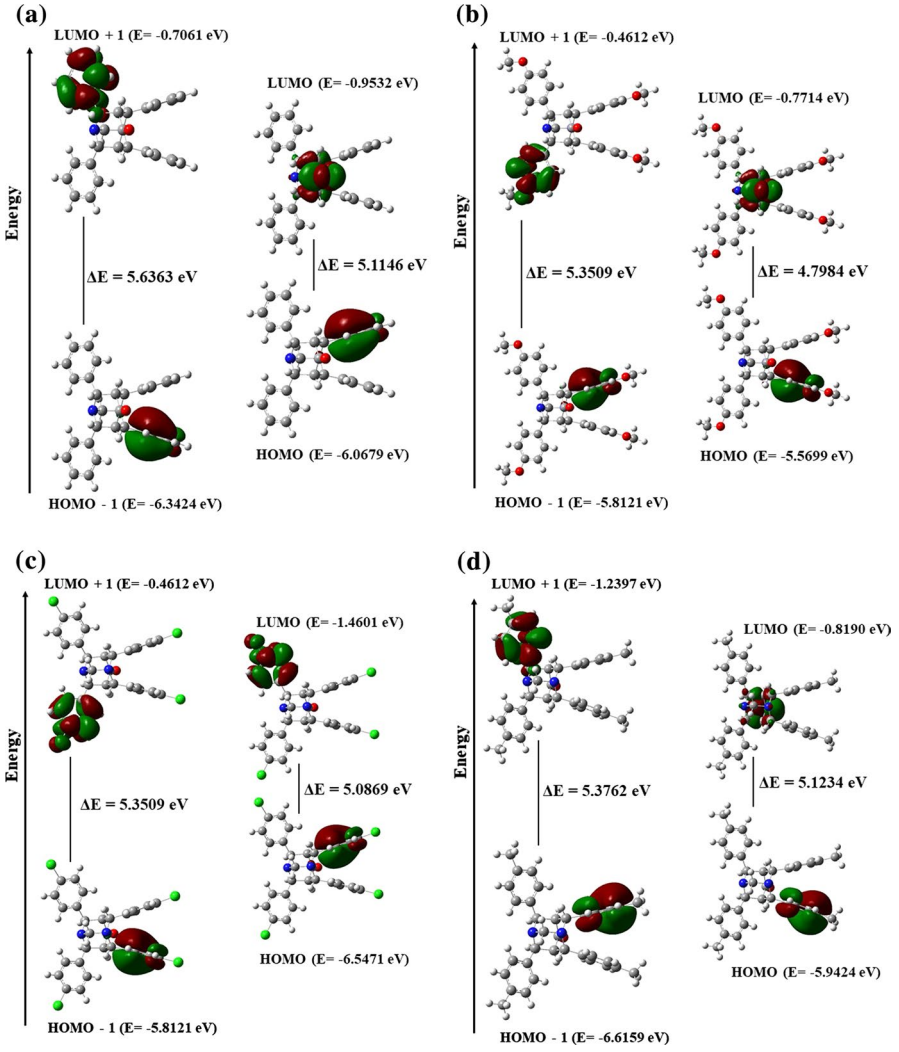

Fig. 4 The HOMO, HOMO-1, LUMO and LUMO+1 orbital of compound **a**–**e**. (**a**) represent compound **a**, (**b**) represent compound **b**, (**c**) represent compound **c**, (**d**) represent compound **d** and (**e**) represent compound **e**

$$\text{Chemical potential}(\mu) = -\frac{(I+A)}{2} \tag{3}$$

$$\text{Electronegativity}(\chi) = \frac{(I+A)}{2} \tag{4}$$

$$\text{Global hardness}(\eta) = \frac{(I-A)}{2} \tag{5}$$

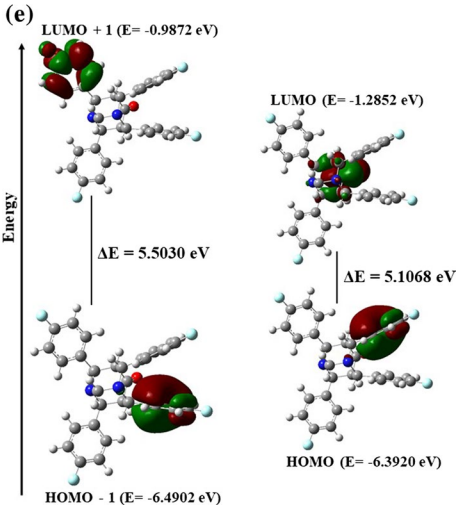

Fig. 4 (continued)

Table 4 HOMO and LUMO energies and the global parameters of synthesized compounds (**a–e**)

Compound	HOMO (eV)	LUMO (eV)	ΔE (eV)	Total energy	μ (eV)	χ (eV)	η (eV)	S (eV)
a	− 6.0679	− 0.9532	5.1146	− 1421	− 3.5105	3.5105	2.5573	0.1955
b	− 5.5699	− 0.7714	4.7984	− 1879	− 3.1706	3.1706	2.3992	0.2084
c	− 6.5471	− 1.4601	5.0869	− 3259	− 4.0036	4.0036	2.5435	0.1965
d	− 5.9424	− 0.8190	5.1234	− 1578	− 3.3807	3.3807	2.5617	0.1951
e	− 6.3920	− 1.2852	5.1068	− 1818	− 3.8386	3.8386	2.5534	0.1958

$$\text{Softness}(S) = \frac{1}{2\eta} \tag{6}$$

In the title compound (**a**–**e**), HOMO is located over any one of the axially oriented aryl rings and LUMO is located over the carbonyl group. In the case of compound **c,** LUMO is located in one of the equatorially orientated aryl rings. The ΔE for the title compounds is around 5.1 eV. The ΔE is higher which confirms that the molecule has a stable structure and also indicates that minimum charge transfer interaction occurs within the molecule [33]. The higher ionization potential demonstrates that, the higher energy is required to remove an electron from the HOMO. The lower value of electron affinity indicates that the molecule easily undergoes an electrophilic reaction. From Table 4, the compound **d** has the highest energy gap value which means the low chemical reactivity (high kinetic stability), while the compound **b** has the lowest value which means the highest chemical reactivity [34, 35]. Electronegativity represents the electron attracting capability of the molecule. The higher the electronegativity, the stronger is the attracting power to accept an electron from a donor molecule. From Table 4, it is observed that electronegativity

of the studied molecules follows the order **c > e > a > d > b**. This result indicates that electron withdrawing group (**c** and **e**) containing compound easily accepts an electron from the acceptor molecule. Chemical potential is related to reactivity and stability of the molecule. The negative chemical potential value shows that the compound is stable. The chemical potential value increases by the substitution of an electron donating group. The highest value of chemical potential, − 3.1706 eV was obtained for the *p*-OCH_3 substituted molecule. The order of the chemical potential in the studied compounds are **b > d > a > e > c**. The unsubstituted molecule has higher total energy compared to the substituted molecule. The order of the total energy in the studied compounds is **a > d > e > b > c**. Higher hardness and lower softness values confirm that the molecule is less polarizable and higher molecular hardness is associated with the molecule [36, 37].

Molecular electrostatic potential

Molecular electrostatic potential (MEP) are three-dimensional diagrams which can be used to visualize the net electrostatic effect produced at that point by total charge density distribution (electron + proton) of the molecule. MEP surface correlates with chemical reactivity (electrophilic, nucleophilic), dipole moments, and the electronegativity of the molecule [38–40]. The MEP is a useful technique for studying the electrostatic interaction with its adjacent groups and surroundings. It is additionally used to predict the reactivity of the molecule towards the biological systems and hydrogen bonding interaction [41]. The different values of the electrostatic potential at the MEP surface are represented by different colors; red and yellow represent regions of more and slightly electron rich electrostatic potential, respectively. The green and blue color represent the region most positive and of zero electrostatic potential, respectively.

As it can be seen from Fig. 5, the red region is mainly localized on a carbonyl group of the ring, showing a most favorable site for the electrophilic attack, the yellow regions are localized on the phenyl groups. In Fig. 5b, for the MEP surface for the methoxy-substituted phenyl ring, the red region is localized on carbonyl and methoxy groups of the compound, with yellow color spread over the phenyl groups. As observed in Fig. 5c and e, the red region is mainly localized on a carbonyl group, the slightly electron rich yellow region localized on fluorine and chlorine atoms, whereas more positive and zero electrostatic potential are localized over the phenyl groups which are most reactive sites for a nucleophilic attack. These results are expected because MEP correlates with electron density and electronegativity of the molecule.

The natural bond orbital (NBO) analysis

The natural bond orbital (NBO) analysis provides an efficient method to understand the various second-order interactions between the filled orbitals of one subsystem and vacant orbitals of another subsystem, which supplement the analysis of both the intra and intermolecular interactions. Computationally calculated localized

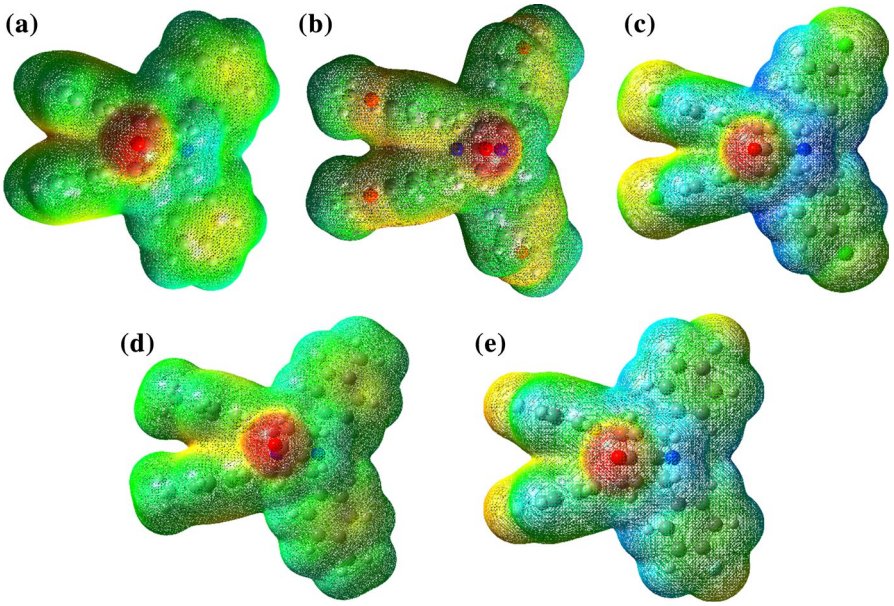

Fig. 5 Molecular electrostatic potential surface of synthesized compounds **a**–**e**

molecular orbitals are used to study the distribution of electron density in atoms, in bonds and in between the atoms. The stabilization energy ($E^{(2)}$) for various conjugative interactions can be obtained from the second order perturbation theory [42]. In NBO analysis the larger the $E^{(2)}$ value, the more intensive is the interaction between electron donors and electron acceptors and the greater the extent of conjugation of the whole system. The intensive interactions are given in the supporting information Table S4–S8. The interaction result is a loss of occupancy from the localized NBO of the idealized Lewis structure into an empty non-Lewis orbital [43, 44]. For each donor, NBO (i) and acceptor NBO (j), the stabilization energy ($E^{(2)}$) associated with electron delocalization i to j is estimated by Eq. (7) [45]

$$E^{(2)} = \Delta E_{ij} = q_i \frac{F(i,j)^2}{\varepsilon_i - \varepsilon_j}, \tag{7}$$

where q_i is the donor orbital occupancy, ε_i and ε_j are diagonal elements, and $F(i,j)$ is the off-diagonal NBO Fock matrix element.

In the compounds (**a**–**e**), NBO analysis shows that strong intermolecular hyperconjugative interaction occurs in π and a lone pair of electrons. The larger the stabilization energy $E^{(2)}$ of the compound, the greater is the stability of the molecule. In the studied compounds, the $E^{(2)}$ value are greater for the delocalization of the electrons between the bond present in the substituted phenyl rings and lone pair electron containing atoms. The lone pair electrons in nitrogen and oxygen atoms are delocalized to nearby antibonding orbitals with high stabilization energy around 19–20 kJ mol^{-1}. A strong intramolecular hyper-conjugative interaction is present within the substituted phenyl rings

with the stabilization energy around 19–22 kJ mol^{-1}. In the studied compounds, two pairs of phenyl rings are present, one pair oriented in the axial position and another pair oriented in the equatorial position. In fluoride, chloride, methoxy substituted compounds, four phenyl rings exhibit two sets of stabilization energy and electron density. This is due to the presence of one pair of phenyl rings in axial positions and another pair of phenyl rings in equatorial positions.

Local reactivity descriptors

The Fukui function gives information about the tendency of a molecule to lose or gain an electron thus predicting which atom in the molecule would be more prone to a nucleophilic or electrophilic attack. It is one of the most broadly used among local reactivity determinants. The Fukui functions such as nucleophilic attack, electrophilic attack, and radical attack have been calculated [46]. The individual atomic charges calculated by Mulliken population analysis (MPA) and B3LYP/6-31G(d,p) level of theory have been used to calculate the Fukui function. Fukui functions are calculated using the following Eqs. (8)–(11),

$$\text{For electrophilic attack } f_j^- = q_j(N) - q_j(N-1), \tag{8}$$

$$\text{For nucleophilic attack } f_j^+ = q_j(N+1) - q_j(N), \tag{9}$$

$$\text{For free radical attack } f_j^0 = [q_j(N+1) - q_j(N-1)], \tag{10}$$

here, q_j is the atomic charge at the jth atomic site, and (N), $(N+1)$ and $(N-1)$ are the total electrons present in the neutral, anion and cation state of the studied molecule, respectively [47]. Morell et al. [48] proposed a dual descriptor ($\Delta f(r)$), which is defined as the difference between the nucleophilic and electrophilic Fukui function and is given by the Eq. (11),

$$\Delta f(r) = \left[f^+(r) - f^-(r)\right]. \tag{11}$$

If $\Delta f(r) > 0$, then the site is favored for a nucleophilic attack, whereas if $\Delta f(r) < 0$, then the site may be favored for an electrophilic attack. The calculated Fukui function values are reported in Table S9–S13. The title compounds are susceptible to more electrophilic attack than the nucleophilic attack. The results of the Fukui function analysis are in good agreement with the MEP results. The isosurface density of the Fukui function for electrophilic attack (f^-) and nucleophilic attack (f^+) is also shown in Fig. 6.

Molecular docking analysis

Molecular docking analysis of 2RLF

The interaction between the ligand and the targeted proteins is presented in Fig. 7. The binding energy, inhibition constant (ki) and reference root mean square

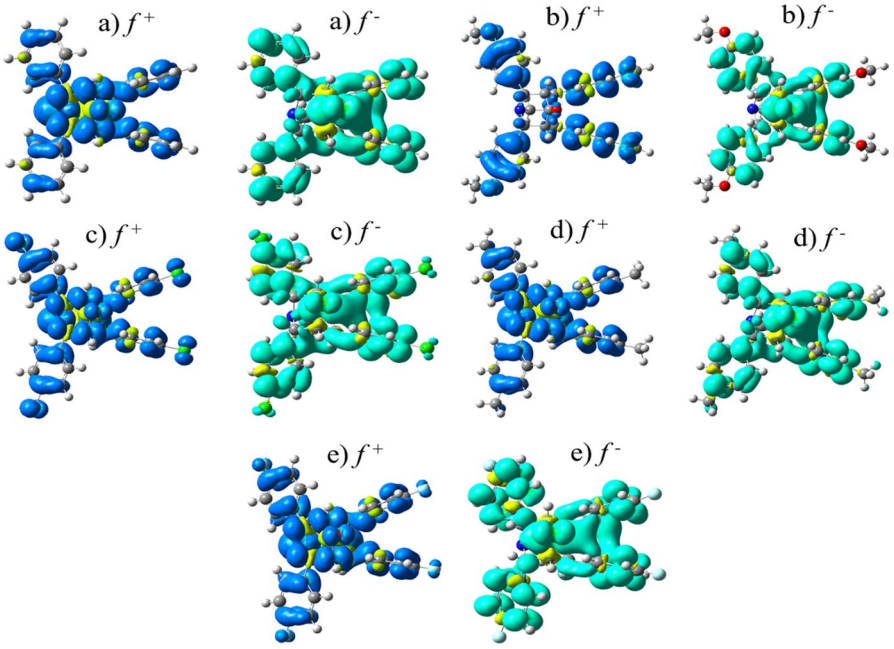

Fig. 6 The nucleophilic Fukui functions (f^+) and electrophilic Fukui functions (f^-) and isosurface density of the studied compounds in the gas phase (isosurface value = 0.03; isosurface density = 0.0004)

deviation (RMSD) are listed in Table 5. The docking results revealed that the synthesized 1, 3-diazaadamantanone derivatives (**a**–**e**) in the binding pocket of 2RLF displayed two types of interactions (π–π and π-sigma interactions). The residues PHE54, PHE55, LYS49, and ILE51 are in close contact with the ligands. Inhibition constant (ki) provides information about the ligand binding affinity to the protein [49]. The result reveals that ligand **a** interacts with 2RLF protein and exhibits the lower inhibition constant (883.62 nM) and lower binding energy (− 8.26 kcal/mol) compared with other ligands (**b, c, d,** and **e**).

It can be seen from Table 5, that the binding interaction of tetraaryl-1,3-diazaadantan-6-one with the H1N1-M2 channel swine virus are much stronger than those with the simple adamantane (amantadine, rimantadine, and memantine). This suggests that the H1N1-M2 channel has lower binding affinities to the simple adamantane, and it may be due to the studied compounds (**a**–**e**) containing π–π and π-sigma interactions.

Molecular docking analysis of 4COX

The interaction between the ligand and the targeted proteins is presented in Fig. 8, and essential parameters are shown in Table 6. Among the ligands (**a**–**e**) studied, ligand **c** exhibited the highest docking score (binding energy—11.13 kcal/mol) and inhibition constant (6.98 nM) in the active site of 4COX. Moreover, the ligands

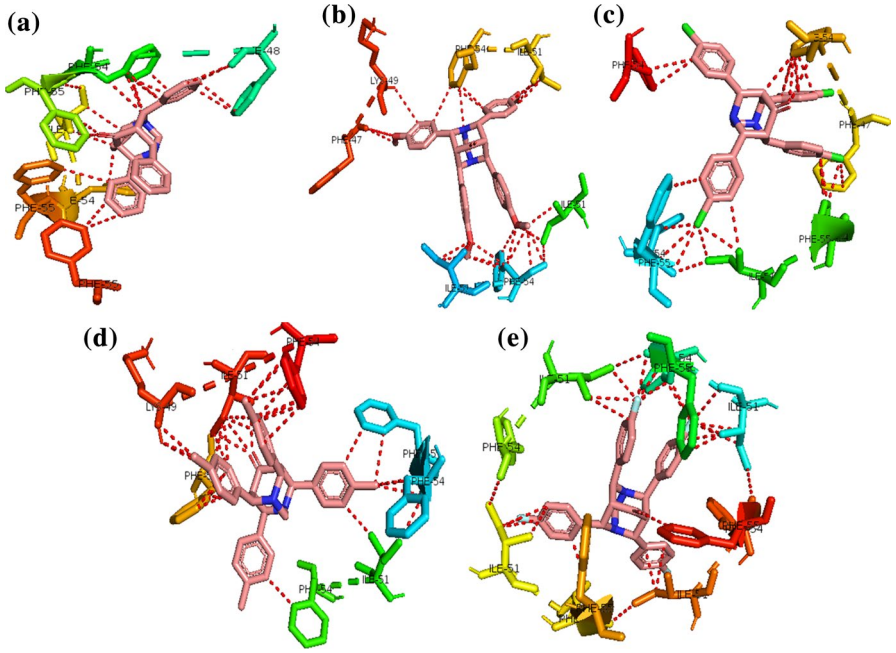

Fig. 7 Molecular docking studies of synthesized compounds (**a**–**e**) against H1N1 swine virus

Table 5 Molecular docking parameters of compound (**a**–**e**) against H1N1 swine virus (2RLF)

Compound	Free energy of binding (kcal/mol)	Inhibition constant, Ki	Reference RMS	Closed content
a	− 8.26	883.62 nM	12.87	PHE55, PHE54, ILE51
b	− 8.22	937.39 nM	11.48	PHE47, ILE51, LYS49, PHE54
c	− 7.43	3.59 µM	12.9	PHE54, PHE47, PHE55, ILE51
d	− 7.43	3.56 µM	11.3	PHE54, PHE55, ILE51
e	− 7.58	2.76 µM	14.44	PHE54, PHE55, ILE51, LYS49
Amantadine[a]	− 4.96	231.93 µM	17.32	PHE, LYS, SER
Rimantadine[a]	− 5.22	150.15 µM	16.67	PHE, LYS, ILE
Memantinea[a]	− 5.52	90.48 µM	16.16	PHE, LYS, SER

[a]Reference compound (simple adamantane)

studied did not demonstrate any hydrogen bond interaction with the active sites of the protein, and it showed the least binding energies, because of π-sigma interactions. This docking post analysis revealed that the compound **c** is oriented with the non-covalent interactions surrounded by the side chains of LEU145 and LEU224 in

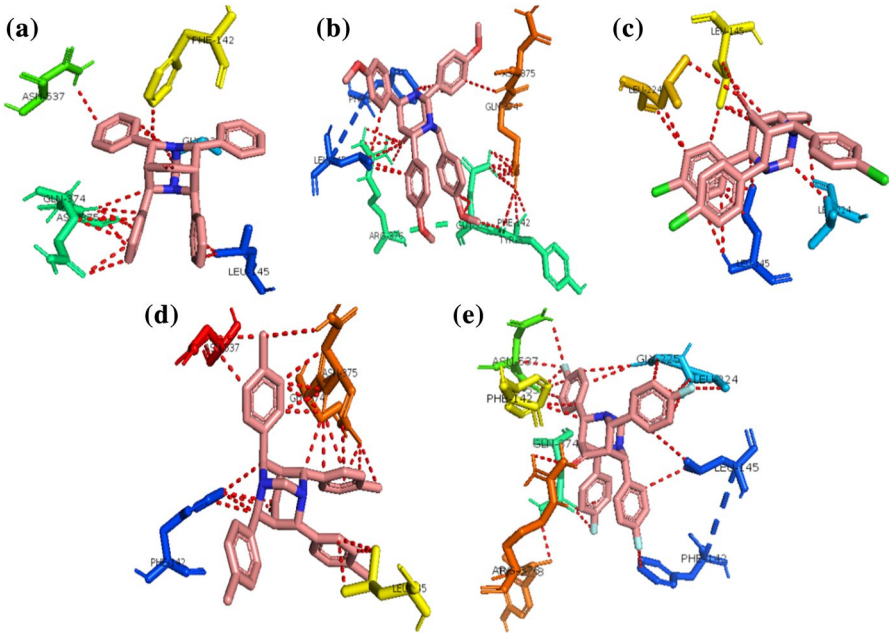

Fig. 8 Molecular docking studies of synthesized compounds (**a**–**e**) against COX–2 protein

the target protein. The interaction of the ligands (**a**–**e**) with studied protein residue are shown in Table 6.

These results in Table 6 reveal that the 4COX protein interaction with tetraaryl-1,3-diazaadantan-6-one (**a**–**e**) exhibits the higher binding energy compared with the simple adamantane (amantadine, rimantadine, and memantine). This may be due to studied compounds (**a**–**e**) exhibiting π–π and π-sigma interactions but in the case of amantadine, rimantadine and memantine this type of interaction is not possible.

Conclusion

In the present investigation, we have synthesized 4,8,9,10-tetraaryl-1,3-diaza-adamantan-6-ones (**a**–**e**) and characterized by FT-IR, ^{1}H and ^{13}C NMR spectra and experimental spectra compared with theoretical spectra. The computed HOMO–LUMO energies with negative values and small orbital energy gap show that the molecule is stable and the molecule readily undergoes electrophilic reaction. The MEP reveals that the phenyl groups and the carbonyl group are the most reactive sites for nucleophilic attack and electrophilic attack, respectively. The NBO investigation demonstrates that a strong interaction exists within the phenyl groups and the lone pair electron of oxygen and nitrogen with the anti-bonding orbitals of carbon atoms. The docking results revealed that the compounds (**a**–**e**) in the binding pocket of 2RLF displayed mainly π interaction with PHE residues. Similarly, the compounds (**a**–**e**) in the binding pocket of 4COX displayed mainly π interaction

Table 6 Molecular docking parameters of compound (**a–e**) against COX–2 protein (4COX)

Compound	Free energy of binding (kcal/mol)	Inhibition Constant, ki	Reference RMS	Closed content with in 3.5 Å
a	− 9.65	83.86 nM	52.96	PHE142, ASN537, GLN374, ASN375, GLY225, LEU145
b	− 9.61	90.51 nM	50.87	TYR373, GLN374, GLY536, LEU145, GLY225, PHE142, ARG376
c	− 11.13	6.98 nM	51.73	LEU145, LEU224
d	− 10.86	10.87 nM	51.03	PHE142, LEU145, ASN375, GLN374, ASN537
e	− 9.27	160.22 nM	51.83	ASN537, PHE142, GLY225, GLN374, TYR373, GLY536, LEU224
Amantadine[a]	− 5.60	78.22 µM	56.23	GLN, PHE, PRO, TYR
Rimantadine[a]	− 6.11	33.07 µM	50.74	GLN, PHE, PRO, HIS
Memantine[a]	− 6.43	19.33 µM	56.36	GLN, PHE, TYR, THR

[a]Reference compound (simple adamantane)

with LEU residue. The synthesized compounds have higher binding energy compared to simple adamantanes. This preliminary result revealed that the compounds (**a**–**e**) might exhibit anti-H1N1 swine virus and anti-COX-2 activity, which will be of use for developing new drugs. However, biological tests should be done to validate the computational predictions.

Acknowledgements The authors thank the UGC, New Delhi for Major Research Project (Grant No. 42-358/2013 (SR)) & UGC-Special Assistance Program (SAP). The authors gratefully acknowledge the DST- FIST NMR facility of Department of Chemistry, Gandhigram Rural Institute-Deemed to be University for recording NMR spectra.

Compliance with ethical standards

Conflict of interest The authors declare that they have no conflict of interest in the manuscript.

References

1. W.L. Davies, R.R. Grunnert, R.F. Haff, J.W. McGahen, E.M. Neumeyer, M. Paulshock, J.C. Watts, T.R. Wood, E.C. Hermann, C.E. Hoffmann, Science **144**, 862 (1964)
2. Y. Togo, R.B. Hornick, A.T. Dawkins, J. Am. Med. Assoc. **203**, 1089 (1968)
3. F.G. Hayden, J.M.I. Gwaltney, C.R.L. Van, K.F. Adams, B. Giordani, Antimicrob. Agents Chemother. **19**, 226 (1981)
4. S. Rabinovich, J.T. Baldini, R. Bannister, Am. J. Med. Sci. **257**, 328 (1969)
5. J. Balzarini, B. Orzeszko, J.K. Maurin, A. Orzeszko, Eur. J. Med. Chem. **42**, 993 (2007)
6. J. Balzarini, B. Orzeszko-Krzesińska, J.K. Maurin, A. Orzeszko, Eur. J. Med. Chem. **44**, 303 (2009)
7. M.A. Al-Omar, E.S. Al-Abdullah, I.A. Shehata, E.E. Habib, T.M. Ibrahim, A.A. El-Emam, Molecules **15**, 2526 (2010)
8. O. Kouatly, A. Geronikaki, C. Kamoutsis, D. Hadjipavlou-Litina, P. Eleftheriou, Eur. J. Med. Chem. **44**, 119 (2009)
9. A.A. Kadi, E.S. Al-Abdullah, I.A. Shehata, E.E. Habib, T.M. Ibrahim, A.A. El-Emam, Eur. J. Med. Chem. **45**, 5006 (2010)
10. G. Zoidis, I. Papanastasiou, I. Dotsikas, A. Sandoval, R.G. Dos Santos, Z. Papdopoolou-Daifoti, A. Vamvakides, N. Kolocouris, R. Felix, Bioorg. Med. Chem. **13**, 2791 (2005)
11. A. Baxter, J. Bent, K. Bowers, M. Braddock, S. Brough, M. Fagura, M. Lawson, T. McInally, M. Mortimore, M. Robertson, R. Weaver, P. Webborn, Bioorg. Med. Chem. Lett. **13**, 4047 (2003)
12. J.C.E. Owen, P.S. Whitton, Brain Res. **1117**, 206 (2006)
13. E.B. Villhauer, J.A. Brinkman, G.B. Naderi, B.F. Burkey, B.E. Dunning, K. Prasad, B.L. Mangold, M.E. Russell, T.E. Hughes, J. Med. Chem. **46**, 2774 (2003)
14. D.J. Augeri, J.A. Robl, D.A. Betebenner, D.R. Magnin, A. Khanna, J.G. Robertson, A. Wang, L.M. Simpkins, P. Taunk, Q. Huang, S. Han, B. Abboa-Offei, M. Cap, L. Xin, L. Tao, E. Tozzo, G.E. Welzel, D.M. Egan, J. Marcinkeviciene, S.Y. Chang, S.A. Biller, M.S. Kirby, R.A. Parker, L.G. Hamann, J. Med. Chem. **48**, 5025 (2005)
15. M.S. Scherman, E.J. North, V. Jones, T.N. Hess, A.E. Grzegorzewicz, T. Kasagami, I.H. Kim, O. Merzlikin, A.J. Lenaerts, R.E. Lee, M. Jackson, C. Morisseau, M.R. McNeil, Bioorg. Med. Chem. **20**, 3255 (2012)
16. A.A. El-Emam, A.M.S. Al-Tamimi, M.A. Al-Omar, K.A. Alrashood, E.E. Habib, Eur. J. Med. Chem. **68**, 96 (2013)
17. E.J. North, M.S. Scherman, D.F. Bruhn, J.S. Scarborough, M.M. Maddox, V. Jones, A. Grzegorzewicz, L. Yang, T. Hess, C. Morisseau, M. Jackson, M.R. McNeil, R.E. Lee, Bioorg. Med. Chem. **21**, 2587 (2013)
18. E.S. Al-Abdullah, H.M. Al-Tuwaijri, H.M. Hassan, M.A. Al-Alshaikh, E.E. Habib, A.A. El-Emam, Molecules **20**, 8125 (2015)

19. L.H. Al-Wahaibi, H.M. Hassan, A.M. Abo-Kamar, H.A. Ghabbour, A.A. El-Emam, Molecules **22**, 710 (2017)
20. G.L. Balaji, S. Sarveswari, V. Vijayakumar, Res. Chem. Intermed. **41**, 6765 (2015)
21. S. Sivasubramanian, M. Sundaravadivelu, N. Arumugam, Org. Prep. Proced. Int. **22**, 645 (1990)
22. V. Vijayakumar, M. Sundaravadivelu, S. Perumal, Magn. Reson. Chem. **39**, 101 (2001)
23. J.F. Wang, D.Q. Wei, K.C. Chou, Biochem. Biophys. Res. Commun. **388**, 413 (2009)
24. K.M. Amin, M.M. Kamel, M.M. Anwar, M. Khedr, Y.M. Syam, Eur. J. Med. Chem. **45**, 2117 (2010)
25. G.M. Morris, D.S. Goodsell, R.S. Halliday, R. Huey, W.E. Hart, R.K. Belew, A.J. Olson, J. Comput. Chem. **19**, 1639 (1998)
26. M.J. Frisch, J.A. Pople, J.S. Binkley, J. Chem. Phys. **80**, 3265 (1984)
27. R. Ditchfield, Mol. Phys. **27**, 789 (1974)
28. C.Y. Panicker, H.T. Varghese, P.S. Nayak, B. Narayana, B.K. Sarojini, H.K. Fun, J.A. War, S.K. Srivastava, C.V. Alsenoy, Spectrochim Acta A **148**, 18 (2015)
29. R.G. Parr, R.G. Pearson, J. Am. Chem. Soc. **105**, 7512 (1983)
30. R.G. Pearson, Proc. Natl. Acad. Sci. USA **83**, 8440 (1986)
31. R.G. Parr, L.V. Szentpaly, S. Liu, J. Am. Chem. Soc. **121**, 1922 (1999)
32. Z. Zhou, R.G. Parr, J. Am. Chem. Soc. **112**, 5720 (1990)
33. D. Mahadevan, S. Periandy, M. Karabacak, S. Ramalingam, N. Puviarasan, Spectrochim. Acta A **86**, 139 (2012)
34. J. Aihara, Theor. Chem. Acc. **102**, 134 (1999)
35. J. Aihara, J. Phys. Chem. A **103**, 7487 (1999)
36. T.K. Kuruvilla, J.C. Prasana, S. Muthu, J. George, S. AnnMathew, Spectrochim. Acta A **188**, 382 (2018)
37. F.A.M. Al-Omary, A. Raj, K. Raju, C. Yohannan Panicker, N.G. Haress, A.A. El-Emam, M.B. El-Ashmawy, A.A. Al-Saadi, C.V. Alsenoy, J. Ahmad War, Spectrochim. Acta A **136**, 520 (2015)
38. E. Scrocco, J. Tomasi, Adv. Quantum Chem. **11**, 115 (1979)
39. E.J. Luque, J.M. Lopez, M. Orozco, Theor. Chem. Acc. **103**, 343 (2000)
40. T. Karthick, P. Tandon, J. Mol. Model. **22**, 142 (2016)
41. J. Lu, W.R. Kobertz, C. Deutsch, J. Mol. Biol. **371**, 1378 (2007)
42. N. Uludağ, G. Serdaroğlu, A. Yinanc, J. Mol. Struct. **1161**, 152 (2018)
43. A. Esme, S.G. Sagdinç, Spectrochim. Acta A **188**, 443 (2018)
44. F. Weinhold, C.R. Landis, E.D. Glendening, Int. Rev. Phys. Chem. **35**, 399 (2016)
45. A.E. Reed, L.A. Curtiss, F. Weinhold, Chem. Rev. **88**, 899 (1988)
46. M. Raja, R. Raj Muhamed, S. Muthu, M. Suresh, J. Mol. Struct. **1141**, 284 (2017)
47. A.O. Zacharias, A. Varghese, K.B. Akshaya, M.S. Savitha, L. George, J. Mol. Struct. **1158**, 1 (2018)
48. C. Morell, A. Grand, A. Toro-Labbe, J. Phys. Chem. A **109**, 205 (2005)
49. S. Sevanthi, S. Muthu, M. Raja, J. Mol. Struct. **1173**, 251 (2018)